Neural-based reconstruction of radioactivity distribution in large water volumes with underwater gliders

Melkon Chatsikian[1], Valsamis Ntouskos[1], Angelos Mallios[2] and Konstantinos Karantzalos[1]

[1]*Remote Sensing Laboratory, National Technical University of Athens, 15772 Zographos, Greece*
[2]*Ploa Technology Consultants S.L., 17003 Girona, Spain*

Abstract

This work focuses on the problem of reconstructing the 3D distribution of radioactivity in large water volumes based on measurements collected with underwater gliders. We present a high-level simulation environment to study radioactivity reconstruction accuracy and efficiency considering different reference radioactivity distributions and under different types of glider trajectories, also taking into account the limitations of radioactivity detection in the water. A neural-based sampling approach is adopted for reconstructing the radioactivity distribution based on the highly sparse measurements.

Keywords

underwater robotics, gliders, radioactivity mapping, environmental intelligence

1. Introduction

Radioactivity, although present in the marine environment, is still significantly undersampled and understudied. Fortunately, water acts as a very effective protective shield against radioactivity emitted from sources deep inside the water, either man-made or natural. Nevertheless, it is important to map radioactivity in underwater environments both because natural radioactivity can be correlated with intense phenomena as earthquakes and volcanic eruptions ([1, 2]), and because the presence of radioactivity in the water (either natural or man-made) can affect the marine biome, with possible environmental and human health risks. For this reason we consider here the possibility to map the distribution of radiation in a large water volume via the detection of gamma radiation in the water using gamma detectors mounted on underwater gliders.

Underwater gliders are underactuated autonomous underwater vehicles, which take advantage of their buoyancy to move through the water [3]. Unlike underwater vehicles that use an engine to create thrust for moving through the water, underwater gliders

AIxIA Artificial Intelligence and Robotics Workshop 2023
melkoncha@gmail.com (M. Chatsikian); ntouskos@mail.ntua.gr (V. Ntouskos); amallios@ploatech.com (A. Mallios); karank@central.ntua.gr (K. Karantzalos)
http://mdouskos.github.io (V. Ntouskos); http://users.ntua.gr/karank/ (K. Karantzalos)
0000-0003-1810-7802 (V. Ntouskos); 0000-0003-1740-5509 (A. Mallios); 0000-0001-8730-6245 (K. Karantzalos)

change their buoyancy and center of gravity, and use their wings to convert vertical motion to horizontal. Different types of sensors can be installed on the gliders, covering a wide range of applications including oceanic research, environmental monitoring, as well as military ones. The most important advantage offered by gliders is their very low energy consumption, as they only require energy to periodically shift slightly their volume and center of gravity to move, allowing them to perform extensively long missions, ranging from days to months, covering very large areas before requiring recharging. Due to these characteristics, underwater gliders are suitable for long surveys, where the ability to remain in the sea for longer periods is more important than the high speed or rapid change of direction offered by other autonomous underwater vehicles. As mentioned above, underwater gliders use the change of their buoyancy, the change of their rudder, and at some cases a minimal thrust from an engine to achieve their motion [4, 5]. Based on these movements, by altering their pitch angle gliders can follow saw-tooth like vertical movements, typically called yo-yos, as well as helical movements with different radii by actuating their ruder at the same time.

In this work, we present a novel high-level simulation environment, which allows to simulate the data collected by gamma radiation detectors mounted on underwater gliders under typical forms of glider trajectories that can be used to scan the volume of interest. To reconstruct the radioactivity distribution in the reference volume based on the sparse measurements, we present a novel interpolation method based on multi-layer perceptrons (MLPs) that is several times more efficient than linear interpolation methods while showing improved accuracy in most cases.

In the following, Section 2 presents a high-level simulation and a novel MLP-based interpolation method developed for studying detection and mapping of radioactivity using underwater gliders, Section 3 discusses the results obtained for a variety of reference radioactivity distributions in the water considering different glider trajectories and interpolation methods, and Section 3 provides concluding remarks.

2. Methodology

For the purposes of this work we consider that measurements from the gamma radiation detectors are stored in tabular format along with the position of the gliders corresponding at the measurement time. Radioactivity mapping considers these data in order to produce a map of the radioactivity distribution in the underwater volume being surveyed. Even without considering uncertainties in the estimated location of the gliders, the problem is notoriously challenging, as measurements cover an infinitesimal portion of the scanned volume. This is inherent to the problem having co-dimension 2, as measurements are virtually 1-dimesional, due to the high locality of the measurements caused by water shielding, and the scanned volume being 3-dimensional. The most obvious solution to propagate measurements to the volume of interest in order to provide a radioactivity map is through interpolation of the recorded values. The simulation environment described next is used to assess the accuracy of the maps reconstructed through interpolation, as well as the efficiency of their calculation. Performing the interpolation using classical

methods, as linear interpolation, leads to very demanding computation due to the very high number of measurements involved and the large extent of the volume needed to be filled. To address these challenges, a novel MLP-based sparse measurement interpolation method is developed, described in the following.

2.1. Simulation environment

A high-level simulation environment has been developed to provide simulated radioactivity measurements given an underlying radioactivity distribution in a reference volume and considering typical trajectories that underwater gliders can execute based on their kinematics. Simplified models are considered both for the radioactivity measurement and the movement of the gliders, not taking into account the efficiency of the gamma radiation detector and the presence of noise regarding the former and not accounting for localization uncertainty regarding the latter. The goal is to provide an environment where different radioactivity detection and mapping scenarios can be tried out, allowing to choose suitable scanning patterns and better understanding limitations due to challenges from radioactivity shielding of the water and the significantly small coverage of the area of interest. The simulator has been developed in Python using the Plotly library, both for the graphical representations, and for the numerical simulations of the measured radioactivity values. A reference volume of interest has been defined in the form of a three-dimensional cuboid with a size of $3000m \times 3000m \times 300m$ (x, y, z axes, respectively) and the simulation is performed in a $1:1$ scale. In this reference volume, two types of underwater glider trajectories are considered. The first corresponds to yo-yo vertical motions, and the other to helical movements, as shown in Figure 1. The simulation considers different spacing between the trajectories. For the yo-yo movement, the horizontal distance between two parallel trajectories is defined as trajectory spacing. For the helical movement, the original volume is divided into smaller sub-volumes with square horizontal section with a given spacing distance. The radius of the helical movement is defined as $1/4$ of the size of this horizontal spacing. The vertical movement of the underwater gliders is limited to the range $25m - 285m$, considering suitable margins for safe operation of the vehicle.

The type of glider trajectory has an important impact on the time required to cover the reference volume and to the total coverage. The simulation environment allows to estimate the time needed to scan the entire volume. Given a specific type of movement, providing the value of the trajectory spacing, the volume is filled with the planned trajectories, allowing to compute the total length of the resulting scan-path. Dividing the scan-path length by the speed of underwater gliders the duration of the scan can be estimated. Additionally, considering a maximum detection range for the radioactivity detectors mounted on the gliders , the volume of the space measured can be estimated in relation to the total scan volume. Table 1 reports indicative scan times and volume coverage estimations for different spacings of the two trajectory types, considering $v = 0.5m/s$ which is a representative value for underwater glider speed and $r_{lim} = 1m$ based on sea water shielding effects affecting radiation detection limit.

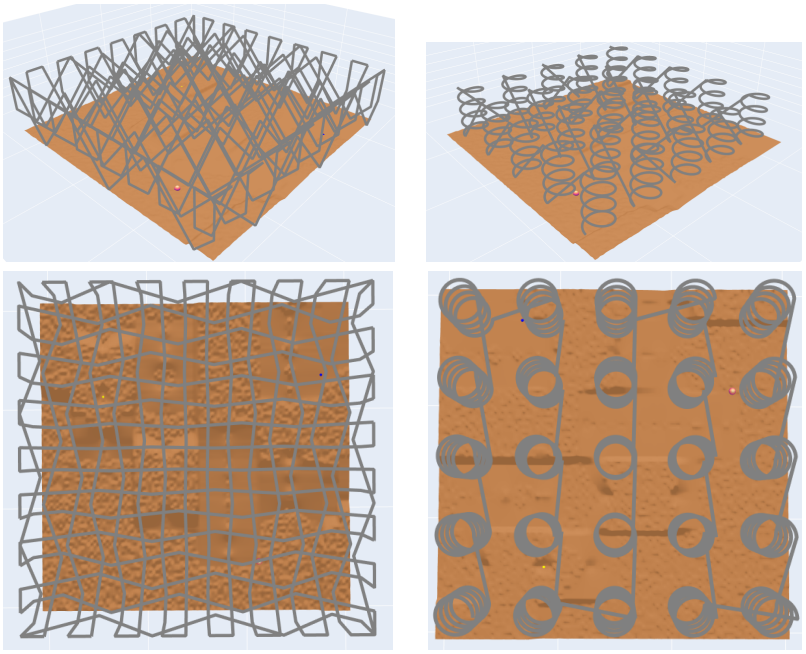

Figure 1: Glider trajectories: vertical yo-yo movements (*Left col.*); helical movements (*Right col.*)

Table 1
Reference volume scan time and coverage for different trajectory spacings.

Yo-yo						Helical					
Spacing (m)	Distance (km)	Scan Time			Coverage (%)	Spacing (m)	Distance (km)	Scan Time			Coverage (%)
100 x 100	221.2	5d	2h	53m	0.025	200 x 200	362.2	8d	9h	13m	0.042
150 x 150	151.8	3d	12h	19m	0.017	300 x 300	229.6	5d	7h	32m	0.026
200 x 200	117.1	2d	17h	2m	0.013	400 x 400	146.7	3d	9h	30m	0.017
250 x 250	96.3	2d	5h	28m	0.011	500 x 500	133.2	3d	2h	0m	0.015

2.2. Radioactivity Distributions

In order to assess the ability of underwater gliders to effectively map underwater radioactivity we consider different radioactivity distributions and use the developed simulator to examine how accurately these distributions can be reconstructed from radioactivity measurements acquired from an underwater glider traversing through them based on different scan trajectories, as described above. Figure 2 summarizes the main types of radioactivity distribution considered. They comprise analytically, geometrically and diffusion based distributions that show different characteristics in terms of shape and spatial frequencies. The first reference distribution is a purely analytical one containing a wide range of spatial frequencies and covering the entire area of interest, defined based on the following relation:

$$I(x,y,z) = \sin\sqrt{\left(\frac{x-1500}{150}\right)^2 + \left(\frac{y-1500}{150}\right)^2 + \left(\frac{z-150}{15}\right)^2}. \quad (1)$$

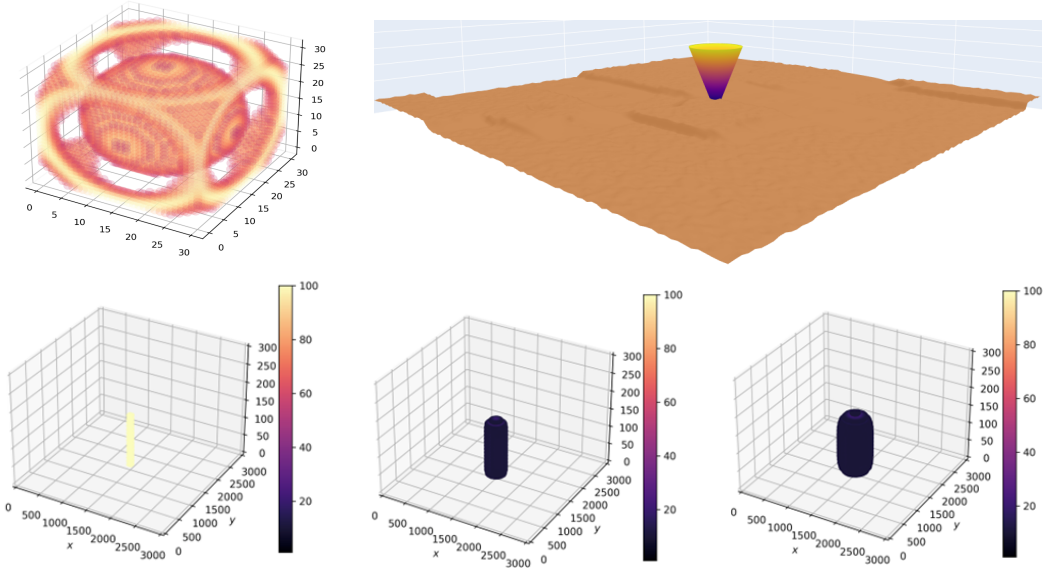

Figure 2: Reference radioactivity distribution. *Top left:* Analytical; *Top right:* Inverted truncated cone representing underwater plume; *Bottom:* Temporal evolution of underwater plum based on Fick's diffusion law visualized at different timesteps

The second reference distribution is a geometrical one described by an inverted truncated cone with a base of $80m$ radius and a top radius of $300m$, approximating the shape of a hydrothermal plume emitted through the center of the volume of interest. The measurements inside the cone are taken as equal to 10 and outside as equal to 1.

The last reference distribution is also approximating a hydrothermal plume, however, considering the diffusion of radioactive material across the vertical column to the surrounding water. Letting J be the diffusion rate, D the diffusion coefficient, C the concentration of the substance and x the distance along the diffusion axis, the radioactivity distribution evolution through time is given based on Fick's second law of diffusion, expressed by [6]:

$$\frac{dC}{dt} = D \cdot \frac{d^2C}{dx^2}. \tag{2}$$

In the simulations, the radioactivity diffusion that corresponds to 4000 timesteps around a cylinder with constant concentration equal to 100 placed in the center of the volume of interest is considered. This results to a radioactivity distribution with values in the range 0 to 100, as can be seen in Figure 2.

2.3. Interpolation

The most straightforward way to reconstruct the radioactitvity distribution based on the values measured along the trajectories is through linear interpolation. Specifically, one

can consider a discretized volumetric representation of the space, according to a spatial sampling distance which defines the dimensions of the resulting voxels. Then, each voxel is filled based on the average of the measurments along the trajectories weighed by the inverse distance to the voxel. It should be noted that even for relatively low measurement rate and spatial resolution(e.g. 1 measurement every $10sec$ and voxels of $\sim 50m$ size) an exact calculation is quite demanding on computational resources, especially in terms of memory.

To better capture the characteristics of the underlying radioactive distribution a non-linear interpolation scheme based on MLPs was considered. The idea of using an MLP for interpolating values from a highly complex function builds on the work of NeRF [7]. In fact, a function of interest can be approximated in arbitrary precision by an MLP, according to the universal approximation theorem [8]. In this context one can optimize the weights of an MLP by providing the function argument as input and using the measured (or computed) value of the function as supervision. In practice, [7] has found that MLPs are not capable of learning high degree functions from low-dimensional inputs. This difficulty can be overcome by applying positional encoding to the input, which artificially increases the dimensionality of the input through the use of Fourier features [9]. In the context of radioactivity mapping, using an MLP as a function approximator and, subsequently as an interpolator through querying values at specific locations, typically leads to an improvement in the accuracy as well as a significant reduction of the required execution time.

3. Results

To assess radioactivity mapping algorithms, the developed simulation environment was used, considering different types of underwater glider trajectories and different radioactivity distributions. A grid of query coordinates was considered consisting of $31 \times 31 \times 8 = 7688$ regularly spaced points. The points are equally spaced in 31 intervals along the x and y axes in the range $[0, 3000]$ and in 8 equally spaced intervals along the z axis in the range $[0, 300]$. The grid size was chosen with the rationale of having enough points to produce a reconstruction accurate and detailed enough, but also with a number of points as small as possible because, as described above, typical implementations (e.g., function 'griddata' of SciPy in Python) are very demanding computationally and an excessive number of query points is prohibitive due to space and time constraints. Table 2 presents the root-mean square error (RMSE) and peak signal to noise ratio (PSNR) metrics, typical metrics used for assessing signal reconstruction quality [10], for the estimated radioactivity maps computed using linear interpolation for yo-yo and helical glider trajectories, respectively.

We note that the radioactivity distribution based on diffusion is better approximated. This can be attributed to the fact that changes in the radioactivity values are quite small. Plume (conical) distribution gives the second-best results, while the analytical distribution of relation (4) is the most challenging, mainly due to the large extent of spatial frequencies that the distribution contains. In terms of the glider trajectories

Table 2
Reconstruction accuracy and computation time for different mapping scenarios considering the yo-yo (*left*) and helical glider movements (*right*).

	Yo-yo					**Helical**			
	Spacing	RMSE	PSNR	Time (sec)		Spacing	RMSE	PSNR	Time (sec)
Analytical	100x100	0.39	14.164	4782	Analytical	200x200	0.20	19.996	9426
	150x150	0.45	12.87	3081		300x300	0.27	17.31	2059
	200x200	0.53	11.61	6601		400x400	0.35	15.07	1697
	250x250	0.53	11.61	2692		500x500	0.37	14.75	894
	300x300	0.56	11.03	2432		600x600	0.39	14.16	1309
Conical	100x100	0.44	26.309	4518	Conical	200x200	0.36	27.863	8904
	150x150	0.45	26.06	3685		300x300	0.45	26.03	2064
	200x200	0.46	25.92	6209		400x400	0.56	24.19	1567
	250x250	0.49	25.37	2474		500x500	0.58	23.76	901
	300x300	0.47	25.73	2490		600x600	0.62	23.27	1350
Diffused	100x100	1.25	37.946	4715	Diffused	200x200	0.97	40.213	9748
	150x150	1.28	37.76	3189		300x300	1.93	34.21	1775
	200x200	1.99	33.92	6514		400x400	1.83	34.66	1692
	250x250	1.47	36.58	2365		500x500	2.90	30.66	863
	300x300	1.76	35.02	2126		600x600	2.73	31.18	1166

used for scanning the volume, the best results are obtained with the helical motion with $200m \times 200m$ spacing, at the cost of excessively long time to complete the mapping. Yoyo-type movement, on the other hand, provides slightly worse results but with the important advantages in terms of reduced scan time. The last column of Table 2 reports the time required to execute the linear interpolation on the $31 \times 31 \times 8$ grid on a typical workstation. This time ranges from 15 minutes to approximately 3 hours. The time required to complete the interpolation task is directly related to the trajectory and the number of query locations. These extended computation times are also one of the reasons of proposing the MLP-based interpolation method.

Regarding MLP-based interpolation, a reference architecture composed of four hidden layers was considered, of which the first three consist of 256 neurons, while the third one consists of 128 neurons. The ReLU activation function was considered for all the hidden layers. The MLP is optimized considering the L_2 loss with respect to the measured values in the corresponding spatial locations. Ten percent of the available data is considered as validation data and an early stopping strategy is implemented, with patience equal to 7 epochs. The early stopping helps to prevent the model from overfitting, thus allowing better approximation of values far from the measured locations. To be able to capture functions with spatial high-frequency components, the three-dimensional input coordinates are transformed using Positional encoding based on Fourier Features [9].

Figure 3, shows the performance comparison of the MLP-based interpolation with respect to the linear interpolation baseline using the PSNR metric, for the yo-yo and helical trajectories. It can be seen that MLP gives comparable performance with the linear based interpolation in the case of yo-yo trajectories, while they lead to significantly better performance when helical trajectories are used. As expected, the smallest sub-

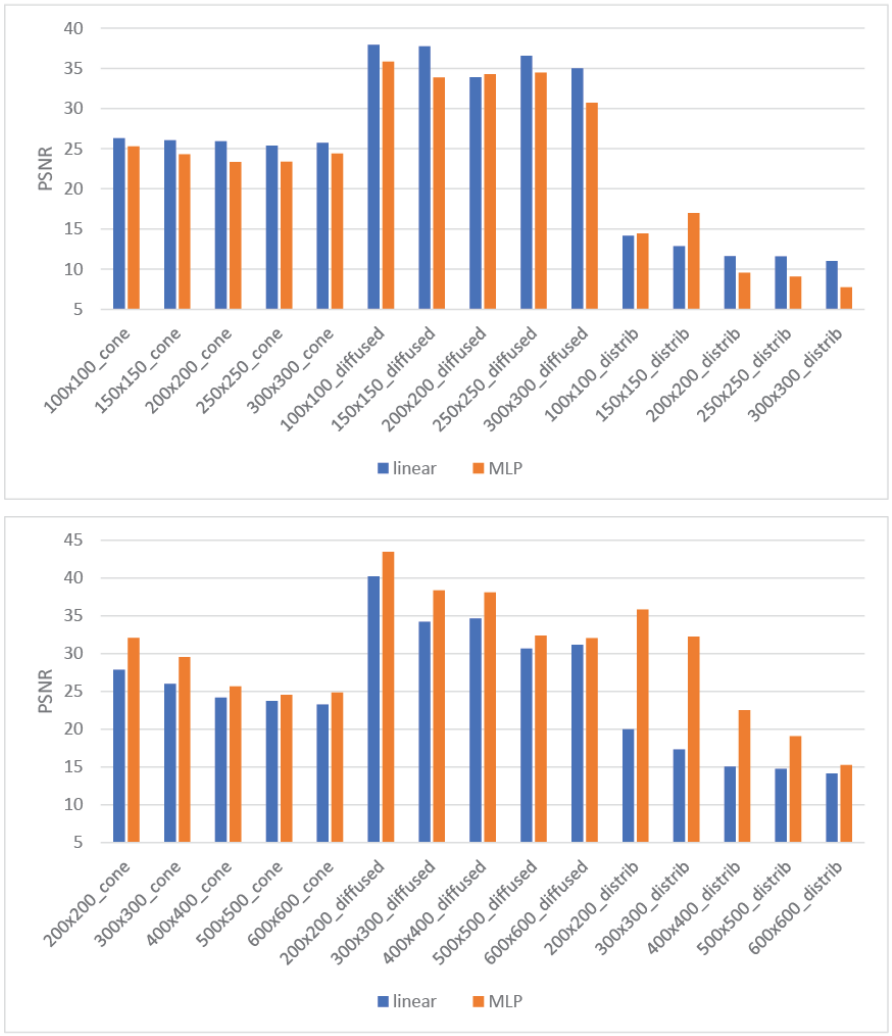

Figure 3: Comparison of radioactivity distribution reconstruction accuracy for linear and MLP-based interpolation for yo-yo (*top*) and helical glider trajectories (*bottom*)

volume spacing, i.e., $200m \times 200m$, leads to the best results. Importantly, the execution time of MLP-based interpolation is sped-up multiple times with respect to linear-based interpolation. In particular, the time required for MLP-based interpolation for the scenarios we considered range from 18 to 369 seconds with an average of 101 seconds. Compared to the corresponding linear interpolation times, this corresponds to a speedup in the worst case of 8 and in the best case of 26 times.

4. Conclusion

A high-level simulation environment has been developed to study the performance of radioactivity mapping based on sparse measurements based on different combinations of glider trajectories, radioactivity distributions and interpolation algorithms. The results are encouraging for the effective mapping of large areas/volumes using glider vehicles, with the simulations suggesting that mapping accuracy depends on the characteristics of the radioactivity distribution, the type and spacing of the scan trajectories, as well as the method used to propagate the measurements to the entire scan volume. Regarding the latter, a novel MLP-based interpolation method has been developed that achieves higher accuracy in most cases with notable speedup with respect to typical linear interpolation implementations. An important outcome of the simulations is that they allow to better understand the trade-off between mapping accuracy and time required to execute the selected scan paths. Finally, although the analysis presented above is based on the characteristics of radioactivity sampling, the developed methodology can be also applied to the 3D mapping of other highly localized physical or chemical quantities of interest in large volumes.

5. Acknowledgments

This work was supported in part by the RAMONES EU H2020 FET-proactive project under Grant 101017808, in part by the iSEAu EU H2020 MSCA-IF project under Grant 101030367, and in part by the SANTORY program funded by the Hellenic Foundation for Research and Innovation under Grant 1850.

References

[1] M. Neri, E. Ferrera, S. Giammanco, G. Currenti, R. Cirrincione, G. Patanè, V. Zanon, Soil radon measurements as a potential tracer of tectonic and volcanic activity, Scientific Reports 6 (2016) 24581.

[2] M. M. Parks, S. Caliro, G. Chiodini, D. M. Pyle, T. A. Mather, K. Berlo, M. Edmonds, J. Biggs, P. Nomikou, C. Raptakis, Distinguishing contributions to diffuse co2 emissions in volcanic areas from magmatic degassing and thermal decarbonation using soil gas ^{222}Rn–$\delta^{13}C$ systematics: Application to santorini volcano, greece, Earth and Planetary Science Letters 377-378 (2013) 180–190. doi:https://doi.org/10.1016/j.epsl.2013.06.046.

[3] M. Y. Javaid, M. Ovinis, T. Nagarajan, F. B. Hashim, Underwater gliders: a review, in: MATEC Web of Conferences, volume 13, EDP Sciences, 2014, p. 02020.

[4] N. Mahmoudian, C. Woolsey, Underwater glider motion control, in: IEEE Conf. on Decision and Control, 2008, pp. 552–557. doi:10.1109/CDC.2008.4739432.

[5] S. Zhang, J. Yu, A. Zhang, F. Zhang, Spiraling motion of underwater gliders: Modeling, analysis, and experimental results, Ocean Engineering 60 (2013) 1–

13. URL: https://www.sciencedirect.com/science/article/pii/S0029801812004325. doi:https://doi.org/10.1016/j.oceaneng.2012.12.023.

[6] A. Fick, V. on liquid diffusion, The London, Edinburgh, and Dublin Philosophical Magazine and Journal of Science 10 (1855) 30–39. doi:10.1080/14786445508641925.

[7] B. Mildenhall, P. P. Srinivasan, M. Tancik, J. T. Barron, R. Ramamoorthi, R. Ng, Nerf: Representing scenes as neural radiance fields for view synthesis, Commun. ACM 65 (2021) 99–106. doi:10.1145/3503250.

[8] A. Pinkus, Approximation theory of the mlp model in neural networks, Acta Numerica 8 (1999) 143–195. doi:10.1017/S0962492900002919.

[9] M. Tancik, P. Srinivasan, B. Mildenhall, S. Fridovich-Keil, N. Raghavan, U. Singhal, R. Ramamoorthi, J. Barron, R. Ng, Fourier features let networks learn high frequency functions in low dimensional domains, in: Advances in Neural Information Processing Systems, volume 33, 2020, pp. 7537–7547.

[10] Z. Wang, A. Bovik, H. Sheikh, E. Simoncelli, Image quality assessment: from error visibility to structural similarity, IEEE Transactions on Image Processing 13 (2004) 600–612. doi:10.1109/TIP.2003.819861.